ORIGINAL RESEARCH ARTICLE

Effect of Nb and Mo on Austenite Microstructural Evolution During Hot Deformation in Boron High Strength Steels

IRATI ZURUTUZA, NEREA ISASTI, ERIC DETEMPLE, VOLKER SCHWINN, HARDY MOHRBACHER, and PELLO URANGA

This work has focused on the study of hot working behavior of boron high strength steels microalloyed with different combinations of Nb and/or Mo. The role of Nb and Mo during the hot deformation of low carbon steels is well known: both mainly retard austenite recrystallization, leading to pancaked austenite microstructures before phase transformation and to refined room temperature microstructures. However, the design of rolling schedules resulting in properly conditioned microstructures, requires microstructural evolution models that take into account the effect of the different alloying elements. In this specific case, the effect that high levels of molybdenum (0.5 pct) have in the recrystallization delay was evaluated. In that respect, hot torsion tests were performed in this work to investigate the microstructural evolution during hot deformation of four boron steels, with different Nb (0.025 pct) and Mo (0.5 pct) combinations. The retardation in recrystallization kinetics was modeled in all cases and measured kinetics agree with those predicted by equations previously developed for Nb–Mo microalloyed steels with lower Mo concentrations (< 0.3 pct). The strain-induced precipitation in the Nb and Nb–Mo bearing steels was also characterized. Finally, the fractional softening evolution during multipass rolling simulations was compared with MicroSim® model predictions, showing a good agreement with experimental results.

https://doi.org/10.1007/s11661-022-06618-0

I. INTRODUCTION

OVER the last years, new alloy concepts as well as innovative thermomechanical processing routes have been developed to fulfill the increasing mechanical property requirements for high-strength steels produced by direct quenching and subsequent tempering treatment. To achieve a good balance between strength and toughness, the combination of boron with microalloying elements (such as Nb, Mo or Nb–Mo) is a common practice.[1–4] Besides selecting an optimum alloy concept, an appropriate design of rolling strategy becomes crucial for achieving pancaked austenite that promotes the formation of refined microstructures and improves resulting mechanical properties. Recently, the effect of combining boron and microalloying elements on phase transformation has been investigated, to select the optimum alloy concept and processing route that ensures the formation of fully martensitic microstructure.[5] Another relevant aspect that has to be considered is the strengthening due to grain size refinement that can be improved reaching a pancaked austenite before phase transformation. It is widely known that the addition of Nb and Mo delays softening kinetics, retards recrystallization of austenite and ensures the accumulation of deformation of the austenite prior to transformation. [6] The addition of Nb and Mo increases the non-recrystallization temperature (T_{nr}) and therefore, the strain is accumulated in austenite during the finishing passes of hot rolling.[7,8] The retardation of the recovery and recrystallization of the austenite is related to the drag effect of Nb and Mo in solid solution and the pinning effect of Nb-rich strain induced precipitates. Depending on the interaction between driving and pinning forces, recrystallization can be partially retarded or fully hindered, promoting the refinement of the transformed room temperature microstructure.[9] Even though the impact of adding Nb and Mo on recrystallization

IRATI ZURUTUZA, NEREA ISASTI, and PELLO URANGA are with the Materials and Manufacturing Division, CEIT-Basque Research and Technology Alliance (BRTA), 20018, Donostia-San Sebastián, Basque Country, Spain and with the Mechanical and Materials Engineering Department, Universidad de Navarra, Tecnun, 20018, Donostia-San Sebastián, Basque Country, Spain. Contact e-mail: puranga@ceit.es ERIC DETEMPLE and VOLKER SCHWINN are with the AG der Dillinger Hüttenwerke, Dillingen, Saar, Germany. HARDY MOHRBACHER is with the NiobelCon BV, 2970 Schilde, Belgium and with the Department of Materials Engineering (MTM), KU Leuven, 3001 Leuven, Belgium.
Manuscript submitted October 15, 2021; accepted January 26, 2022. Article published online February 18, 2022

kinetics was already investigated, the complex interaction between B, Nb and Mo, with higher molybdenum levels, and its effect on the austenite evolution during hot working is still unclear.

In the current work, different types of torsion tests were performed to analyze the interaction between recrystallization and precipitation kinetics for different high-strength medium carbon steels. In addition to evaluate the impact of chemical composition (synergy between B, Nb, Mo and Nb–Mo) and deformation temperature on static recrystallization of austenite, the competition between recrystallization, atoms in solid solution and strain-induced precipitates were analyzed during multipass deformation under continuous cooling conditions (in terms of T_{nr}). Finally, the applicability of the available austenite evolution models was studied.

II. MATERIALS AND METHODS

Table I shows the chemical composition of the studied steels containing 0.16 pct of C and 20 ppm of boron. Laboratory casts were produced for the present work. A reference CMnB steel was selected in addition to three different microalloyed steels with Nb, Mo and NbMo. Nb level is of 0.026 pct and Mo content about 0.5 pct. All the steels are alloyed with Ti to ensure the full effect of boron. All the grades show Ti/N ratios higher than the Ti/N stoichiometric ratio (Ti/N = 3.42).

Two different types of torsion tests were performed in a computer controlled torsion machine. Double twist torsion tests were carried out to define static recrystallization kinetics and multipass torsion tests in order to determine the evolution of fractional softening and the non-recrystallization temperature (T_{nr}). The torsion specimens are characterized by a central gauge section of 17 mm in length and a diameter of 7.5 mm.

The thermomechanical schedule shown in Figure 1 was defined for the double-twist torsion tests. In all cases, a soaking treatment was applied at 1200 °C for 10 minutes, for dissolving microalloying elements. Afterwards, deformation pass of 0.3 was applied at 1175 °C with the aim of refining the initial austenite grain size. After this deformation, the samples were cooled down to the deformation temperature. Two deformation passes were applied in the temperature range between 1100 °C and 850 °C and different interpass times were applied to evaluate the softening fractional evolution. Softening kinetics were recorded for a strain of 0.3. The full softening curve was obtained for the entire range of deformation temperatures (1100 °C, 1000 °C, 950 °C, 900 °C and 850 °C). The fractional softening (FS) for each condition was determined using the 2 pct offset method. It has been reported that, in the absence of strain-induced precipitation, this method excludes adequately the contribution of recovery to the overall softening.[10,11] Torsion double twist technique shows several advantages when compared to the traditional double-hit compression tests.[12] In addition, the initial austenite grain size (D_0) before the double twist torsion tests was measured. To that end, the samples were quenched after reheating and applying a roughing pass at 1175 °C.

For the multipass torsion tests, the thermomechanical schedule included a soaking treatment at 1200 °C for 10 minutes. For CMnB and CMnNbB steels, 24 deformation passes were applied at decreasing temperatures in the 1100 and 640 °C range. For the steels containing Mo, deformation passes were applied from 1200 °C. The temperature decrease between passes was of 20 °C. Different strain per pass of 0.2 and 0.3 and interpass times of 5 and 15 seconds were selected. A strain rate of 1 s^{-1} was defined. The non-recrystallization temperature was defined considering the standard method proposed by Bai *et al.*[13] Fractional softening calculated from the multipass torsion tests were compared with the Micro-Sim-PM® software results which simulates the microstructural evolution of austenite grain size distributions during hot working processes.

The specimens were characterized metallographically in the sub-surface longitudinal section, corresponding to 0.9 of the outer radius of the torsion specimen. The analysis of the austenitic structure was performed using optical microscopy (OM, LEICA DM15000 M, Leica microsystems). The specimens were etched by a solution of saturated picric acid and HCl to reveal the austenite grain boundaries in the quenched samples. Austenite grain size distributions were measured taking into account the mean equivalent diameter method. The measurements were carried out using the QWin v.2.3 image analysis software. For each steel grade, 400 to 600 austenite grains were measured. Concerning the analysis of softening kinetics, in selected conditions, the interaction between strain induced precipitation and recrystallization was analyzed. The study of the fine precipitates was performed using a transmission electron microscope (TEM, JEOL 2100) with a voltage of 200 kV and LaB_6 thermionic filament. To that end, carbon extraction replicas were obtained and strain induced precipitation analysis was carried out.

III. RESULTS AND DISCUSSION

A. *Softening Kinetics*

In Figure 2 the effect of chemical composition on the fractional softening curves for each deformation temperature can be evaluated. The kinetics of static recrystallization defined by an Avrami-type equation[14] is used to fit the experimental data:

$$X_{REX} = 1 - \exp\left(-0.693\left(\frac{t}{t_{0.5}}\right)^{n}\right) \qquad [1]$$

The softening fraction (FS) can be replaced by the recrystallized fraction (X_{REX}), where t is the interpass time, $t_{0.5}$ is the time corresponding to 50 pct of the recrystallized volume and n is the Avrami exponent.

Several approaches for predicting the time of 50 pct recrystallization can be found in the literature. In a previous work,[7] the following equation was deduced for low carbon Nb and Nb–Mo microalloyed steels

Table I. Chemical Composition of the Studied Steels (Wt. Pct)

Steel	C	Si	Mn	Mo	Nb	B	Ti	N	Ti/N
CMnB	0.15	0.32	1.05	0.020	0.0003	0.0022	0.019	0.0051	3.70
CMnNbB	0.16	0.29	1.05	0.020	0.026	0.0019	0.022	0.0052	4.32
CMnMoB	0.16	0.28	1.07	0.51	0.0006	0.0022	0.025	0.0053	4.63
CMnNbMoB	0.16	0.31	1.08	0.52	0.026	0.0018	0.019	0.0052	3.74

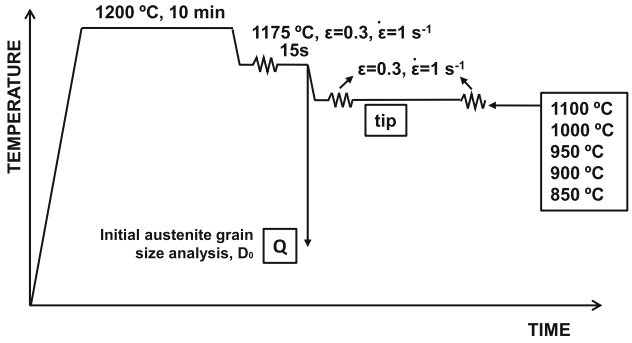

Fig. 1—Schematics of the thermomechanical cycles applied for the softening kinetics.

taking the effect of microalloying elements in solid solution, the deformation parameters (ε, $\dot{\varepsilon}$, and T, strain, strain rate (s^{-1}) and temperature (K), respectively) and the initial austenite grain size (D_0) into account.

$$t_{0.5} = 9.92 \times 10^{-11} \cdot D_0 \cdot \varepsilon^{-5.6D_0^{-0.15}} \cdot \dot{\varepsilon}^{-0.53} \cdot \exp\left(\frac{180,000}{RT}\right) \cdot \exp\left[\left(\frac{275,000}{T} - 185\right) \cdot [\mathrm{Nb}]_{\mathrm{eff}}\right] \quad [2]$$

$$[\mathrm{Nb}]_{\mathrm{eff}} = [\mathrm{Nb}] \text{ for Nb microalloyed steels.}$$

$$[\mathrm{Nb}]_{\mathrm{eff}} = 1.19[\mathrm{Nb}] + 0.09[\mathrm{Mo}] \text{ for 0.03 pct Nb-Mo microalloyed steels.}$$

$$[\mathrm{Nb}]_{\mathrm{eff}} = 1.19[\mathrm{Nb}] + 0.032[\mathrm{Mo}] \text{ for 0.06 pct Nb-Mo microalloyed steels.}$$

The equation was developed for Nb and Nb-Mo low carbon (0.05 pct C) microalloyed steels with Nb content between 0.03 and 0.06 pct and Mo content between 0 and 0.31 pct. The approach includes a Nb effective term that considers the synergy between Nb and Mo in the delaying of recrystallization kinetics. The term related to Mo differs depending on the Nb content. For 0.03 pct Nb this term is about 0.09 and when Nb is increased to 0.06 pct, the Mo effect is reduced significantly, as the term decreases to 0.032. Therefore, the impact of Mo is reduced with increasing Nb content.

From the softening curves, the $t_{0.5}$ and the Avrami exponent n were calculated for the different deformation temperatures and steel grades. Additionally, the initial mean austenite grain sizes (D_0) were also quantified. In Table II the experimental $t_{0.5}$ and n values determined from the softening curves, as well as D_0 measurements have been summarized. Concerning the initial mean austenite grain sizes (D_0), no significant differences are observed in the different steels. Mean initial grain sizes of 47, 59, 49 and 52 μm are measured for CMnB, CMnNbB, CMnMoB and CMnNbMoB steels, respectively.

As shown in Figure 2, for all deformation temperatures, the addition of microalloying elements affects the recrystallization kinetics. This effect is more pronounced as the deformation temperature decreases. In addition, Figure 2 suggests that the decrease of the deformation temperature promotes the delay of softening kinetics. Longer times are required for achieving fully recrystallized austenitic structure. When microalloying elements are added (Nb, Mo or Nb-Mo), even though very long times are applied (see Figures 2(d) and (e)), recrystallization is not completed for the lowest deformation temperatures of 900 °C and 850 °C. At the lowest deformation temperature of 850 °C, recrystallization interacts with deformation induced precipitation and atoms in solid solution in the steels containing Nb (CMnNbB and CMnNbMoB, see Figure 2(e)). However, in the CMnMoB steel, the retardation of the recrystallization kinetic is mainly attributed to the presence of Mo in solid solution. In the CMnNbB and CMNbMoB grades, a plateau can be detected in the fractional softening curve if a deformation temperature of 850 °C is applied (see Figure 2(e)). This plateau is related to the presence of strain induced Nb precipitates that interact with recrystallization kinetics.[15,16]

In Figure 3 the relation between predicted $t_{0.5}$ values by means of Eq. [2] and the experimental value is plotted for the current steels and deformation temperatures. The results indicate that reasonable prediction could be achieved in most cases considering the equation proposed by Pereda *et al.*[7] The R2 score calculated for this dataset is of 0.77.

B. *Analysis of Strain Induced Precipitates*

Precipitation analysis was performed in the quenched samples for Nb and NbMo grades (deformation temperature of 850 °C and interpass time of 300 seconds), in order to confirm that the delaying of recrystallization can be justified by the presence of deformation induced precipitates in austenite. In Figure 4 several TEM images are presented at different magnifications for both Nb microalloyed steels (CMnNbB in Figures 4(a) through (c) and CMnNbMoB in Figures 4(d) through

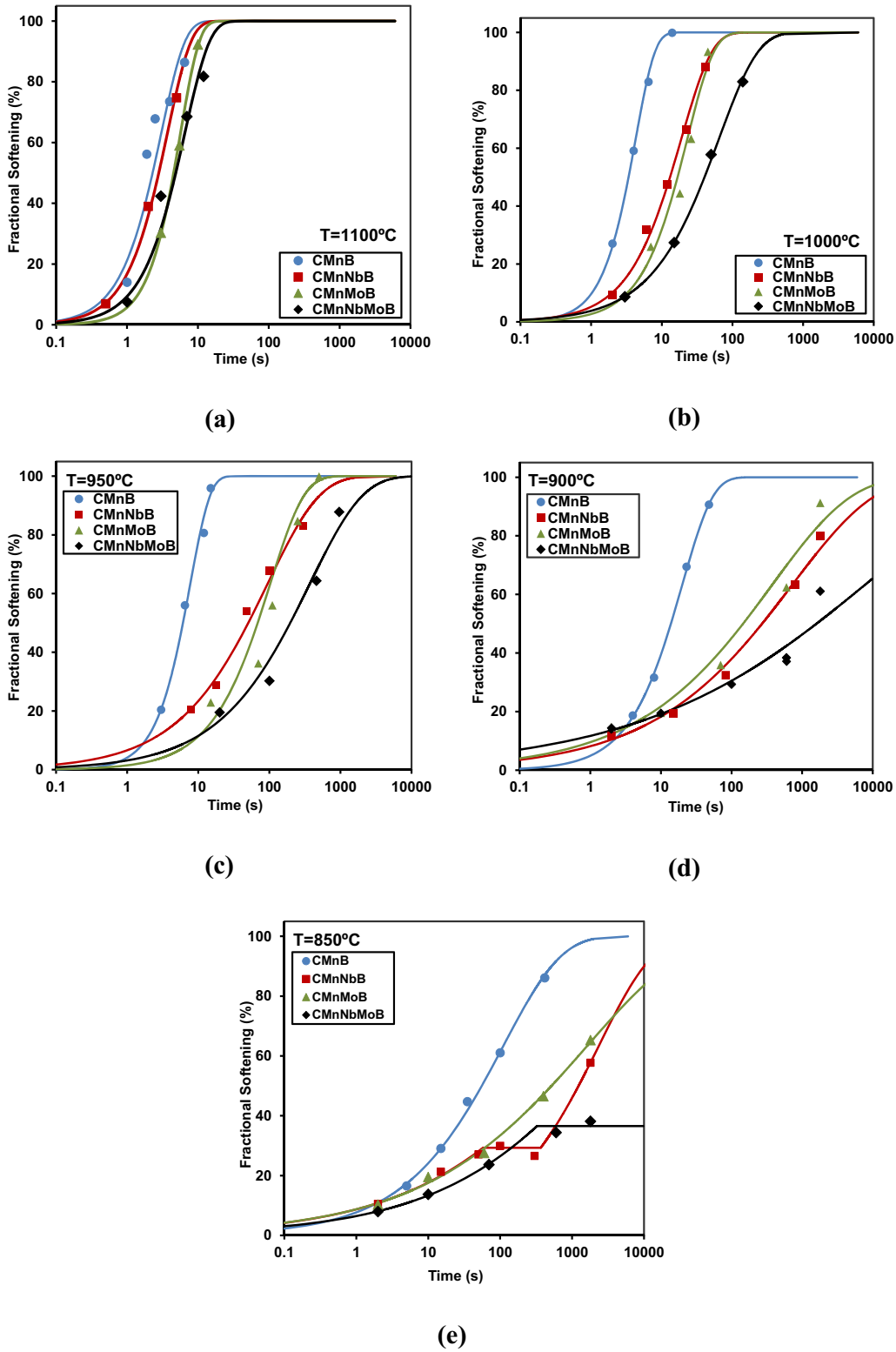

Fig. 2—Effect of the chemical composition on the softening behavior at (*a*) 1100 °C, (*b*) 1000 °C, (*c*) 950 °C, (*d*) 900 °C and (*e*) 850 °C.

(f)). Different precipitate populations can be identified in both chemistries. In addition to non-dissolved Nb and Ti rich precipitates sized between 20 and 50 nm (see Figures 4(a) and (d)), finer strain induced precipitates are also observed (size below 10 nm, as shown in Figures 4(b), (c), (e) and (f)). Spectral analysis (Figure 4(g)) reveals that these strain-induced precipitates are rich in Nb. These fine-sized Nb-based precipitates appear when deformation at low temperatures is applied. Their pinning effect on the austenite grain

Table II. Experimental $t_{0.5}$ and n Avrami Exponent Values, as Well as Initial Austenite Grain Sizes (D_0) Measured at Different Deformation Temperatures and Steel Grades

Steel	ε	D_0 (μm)	T_{def} (°C)	$\dot{\varepsilon}$ (s^{-1})	$t_{0.5}$ (s)	n
CMnB	0.3	47 ± 2	1100	1	2.3	1.3
	0.3		1000		3.4	1.6
	0.3		950		6.1	1.6
	0.3		900		7.7	1.0
	0.3		850		9.6	0.5
CMnNbB	0.3	59 ± 3	1100	1	2.8	1.3
	0.3		1000		13	1.0
	0.3		950		51	0.6
	0.3		900		70	0.4
	0.3		850		—	0.3
CMnMoB	0.3	49 ± 2	1100	1	4.6	1.6
	0.3		1000		17	1.1
	0.3		950		69	0.9
	0.3		900		95	0.5
	0.3		850		127	0.2
CMnNbMoB	0.3		1100		4.9	1.2
	0.3		1000		41	0.8
	0.3	52 ± 3	950	1	196	0.6
	0.3		900		273	0.2
	0.3		850		—	0.3

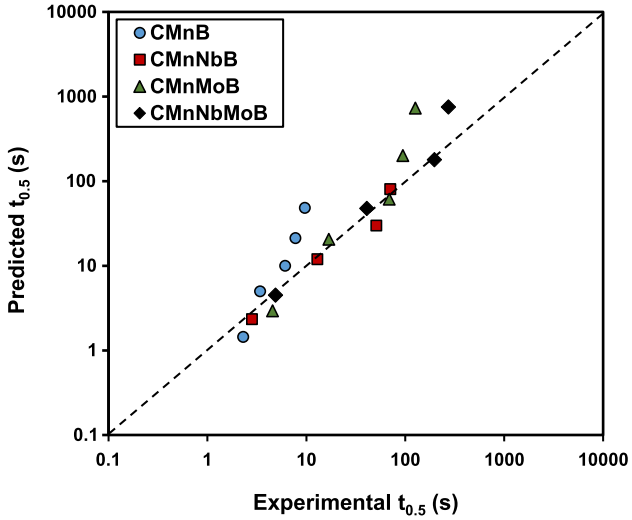

Fig. 3—Comparison between experimental and predicted time of 50 pct recrystallization ($t_{0.5}$) using Eq. 2.

boundaries causes a strong delay of the recrystallization kinetics and augments strain accumulation in austenite prior to transformation.

C. *Multipass Torsion Tests*

1. *Definition of non-recrystallization temperature (T_{nr})*

Multipass torsion tests were performed for two different deformation strains of 0.2 and 0.3 and interpass times of 5 and 15 seconds. The non-recrystallization temperature (T_{nr}) value was defined by means of multipass torsion tests for all the steel grades. Stress strain curves obtained from the torsion tests allowed calculating the mean flow stress (MFS), defined as the area under the stress-strain curve divided by the pass strain, by numerical integration. The MFS for each deformation pass is plotted against the temperature in Figure 5 for an interpass time of 15 seconds. Thereby, the influence of the chemical composition of the steels on the MFS becomes apparent for both deformation strains. Two different regimes can be distinguished. In the initial regime at higher austenite temperature, complete recrystallization takes place between passes and the stress increase from pass to pass is only related to decreasing temperature and accordingly increasing yield strength of austenite. The second regime at lower austenite temperature is indicating strain accumulation caused by incomplete recrystallization.[13] Following the standard procedure,[10] the non-recrystallization temperature (T_{nr}) was determined as the intersection of linear fitted regression lines for the data points of either regime. Thus, non-recrystallization temperatures of 918 °C, 956 °C, 1003 °C and 1015 °C have been determined for CMnB, CMnNbB, CMnMoB and CMnNbMoB steels respectively, when a deformation of 0.2 and t_{ip} of 15 seconds is applied (see Figure 5(a)). An increase on the non-recrystallization temperatures is found for the higher deformation strain of 0.3. Steels with molybdenum alloying comprise the highest T_{nr} values especially when combined with Nb microalloying. Moreover, the molybdenum alloyed variants show a stronger impact of the deformation strain on the T_{nr} values. T_{nr} values measured for the different deformation conditions and all chemistries are summarized in Table III. For both interpass times, the lowest T_{nr} value was achieved for CMnB grade, followed by CMnNbB, CMnMoB and CMnNbMoB steels respectively. The reduction of interpass time, leads to higher T_{nr} values. This trend is observed for both deformation values.

These alloying effects on the non-recrystallization temperature may be related to two mechanisms being solute drag and particle pinning effect caused by strain induced precipitates. Molybdenum, niobium and titanium have a significantly larger atom size than iron and a tendency for segregating towards the austenite grain boundary. The drag effect by the alloying element is enhanced when the solute alloy atom has a large misfit with the matrix atom (Fe) and its self-diffusion coefficient is small. Calculations based on density functional theory have revealed furthermore that large-sized solute atoms have a high binding energy with the austenite grain boundary.[17] This binding energy correlates with the activation energies necessary for static and dynamic recrystallization.[18,19] Of the alloying elements considered in the current steels, niobium has the strongest binding energy followed by molybdenum and titanium. However, the solute drag effect also scales with the number of atoms, at least until saturation of the available grain boundary sites is reached. In that respect molybdenum clearly offers the greater potential since the element has much better solubility in austenite as compared to niobium and titanium having a similarly low solubility. Boron, being a smaller element, shows a lower binding energy.[20–22] Some authors have also reported complex interactions between Nb and B affecting the recrystallization kinetics of Nb.[23] In the

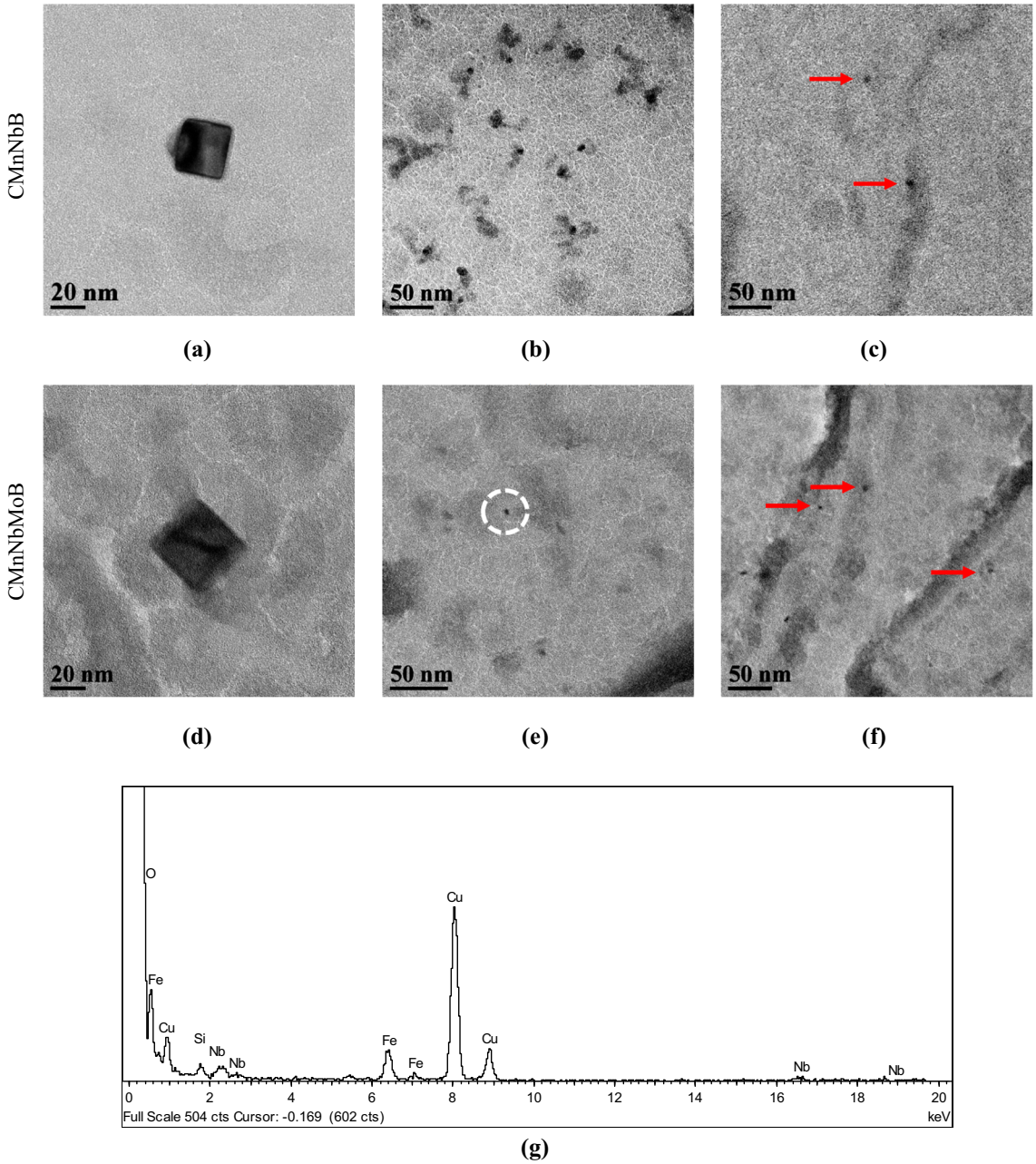

Fig. 4—Nb containing precipitates detected in the carbon replicas extracted from (*a*, *b*, *c*) CMnNbB and (*d*, *e*, *f*) CMnNbMoB steels after a deformation pass in 850 °C (interpass time of 300 s). (*g*) Microanalysis of the fine precipitate marked in (e) in a circle (the presence of Cu in the spectrum is due to the Cu grid of the carbon replica).

current paper, no effect of boron in static recrystallization kinetics was considered.

On the contrary, molybdenum by itself cannot form carbide precipitates in austenite contrary to niobium and titanium. In-situ formation of strain-induced precipitates exerts a pinning effect on austenite grain boundaries according to the well-known Zener theory.[24] As already mentioned, the considered alloying elements (Mo, Nb, Ti) segregate towards austenite grain boundaries with decreasing temperature supported by the flow of vacancies.[25,26] This leads to locally considerably higher concentration of these elements. Interstitial carbon and boron atoms show a similar boundary segregation. Accordingly, the local solubility product of especially niobium can largely exceed the solubility limit facilitating strain-induced precipitation in the immediate boundary neighborhood. Titanium in the current steels is mostly consumed by forming TiN or Ti,Nb(C,N) particles after solidification.[27] The near-stoichiometric (Ti/N) addition of titanium therefore leaves only a small amount available for forming strain-induced Ti particles (Table I). This residual Ti amount is largest in the CMnMoB steel being approximately 60 mass ppm while it is only 15 mass ppm in the CMnNb steel.

Based on these two mechanisms the measured T_{nr} values in Table III can be interpreted. In the CMnB steel

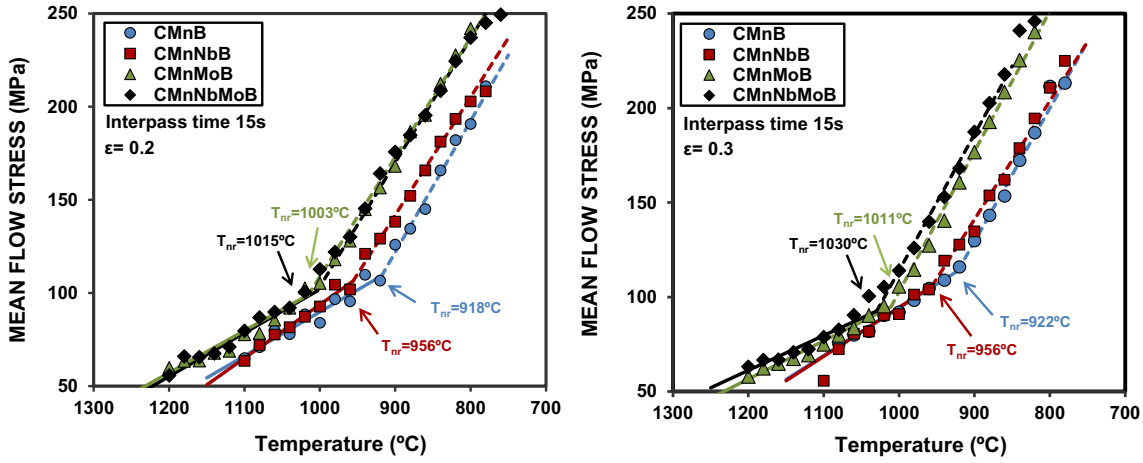

Fig. 5—Mean flow stress derived from multipass torsion tests as a function of temperature for (*a*) 0.2 and (*b*) 0.3 strain levels and an interpass time of 15 s.

Table III. T_{nr} Measured From Multipass Torsion Tests for Both Interpass Times (5 and 15 s), Both Deformation Levels (0.2 and 0.3) and All Chemical Compositions

Steel	Interpass Time (s)	ε	T_{nr} (°C)	Interpass Time (s)	ε	T_{nr} (°C)	ΔT_{nr} (5/15)
CMnB	5	0.2	955	15	0.2	918	37
	5	0.3	947	15	0.3	922	25
CMnNbB	5	0.2	980	15	0.2	956	24
	5	0.3	984	15	0.3	956	28
CMnMoB	5	0.2	1010	15	0.2	1003	7
	5	0.3	1030	15	0.3	1011	19
CMnNbMoB	5	0.2	1024	15	0.2	1015	9
	5	0.3	1049	15	0.3	1030	19

the formation of carbide particles is unlikely since only a very small residual amount of Ti is present. Therefore, any delay of recrystallization must be related to solute drag by the two segregating interstitials carbon and boron. With longer interpass time, this drag effect is increasingly overcome leading to considerably lower T_{nr}. The higher pass strain increases the driving force for recrystallization yet this effect on the T_{nr} is rather small especially for the longer interpass time. The addition of niobium increases T_{nr} considerably by around 35 °C for both interpass times. It is reasonable to assume that for the shorter interpass time the contribution by solute drag is more relevant. The longer interpass time facilitates the formation of precipitates exerting an additional pinning effect while the solute drag effect diminishes. The addition of molybdenum results in a very significant increase of T_{nr} as compared to the CMnB steel. This must be related to strong solute drag due to the rather high amount of solute molybdenum in this steel. Additionally, an influence of the pass strain is evident especially for the shorter interpass time. This could be explained by the higher defect density induced by the larger pass strain facilitating a more pronounced segregation of molybdenum atoms towards the grain boundary. The solute drag effect caused by Mo is also sustained for the longer interpass time reflecting in a smaller decrease of T_{nr} relative to the Mo-free steels. By adding niobium and molybdenum in combination T_{nr} is further increased. This can be attributed to the solute drag effect of niobium.[28] However, the incremental increase in T_{nr} by Nb in the Mo-alloyed is smaller than in the Mo-free steel. It is uncertain whether niobium precipitation already occurs at the generally higher T_{nr} temperatures of the Mo-alloyed steel. The small amount of residual titanium in these steels does not appear to have a significant influence on the recrystallization behavior.

2. *Comparison between experimental anisothermal fractional softening and predicted by MicroSim® model*

The experimental work was complemented by the advanced modeling tool MicroSim-PM®. This plate mill model allows predicting the evolution of austenite conditioning and can be a very useful tool for designing the optimum combination of rolling schedule and alloy composition.[29] In the present study MicroSim-PM® software was used for predicting the recrystallized fraction of austenite from pass to pass and estimating

the evolution of Fractional Softening (FS) during plate hot rolling simulation. This analysis supports the understanding of the mechanisms involved and the interaction between precipitation and recrystallization in each alloy composition. MicroSim-PM® requires the initial austenite grain size distribution as an input and returns the size distributions for recrystallized and unrecrystallized fractions at the onset of subsequent rolling passes. For that purpose, the model assumes the interaction between different mechanisms acting during the interpass time, such as, static and metadynamic recrystallization, grain growth and Nb(C,N) strain induced precipitation. The equations implemented in the model are developed from industrially produced plates for plain CMn, Nb and NbMo microalloyed steels and adapted for a wide range of initial austenite grain sizes.

The fractional softening curves predicted by the model for the various steel compositions are plotted as a function of temperature for a deformation strain of 0.3 and an interpass time of 15 seconds in Figure 6. In addition, based on the results extracted from the multipass torsion tests, experimental FS results are overlayed in each graph for comparison. For determination of the fractional softening, anisothermal interpass conditions were assumed, considering the approach proposed by Liu and Akben[30] shown in Eq. [3].

$$\text{FS (pct)} = \frac{\sigma_m^i - \sigma_y^{i+1}\frac{\sigma_0^i}{\sigma_0^{i+1}}}{\sigma_m^i - \sigma_0^i} \cdot 100 \qquad [3]$$

where σ_m^i and σ_y^{i+1} are the maximum and the yield stresses for both, the ith (at temperature T_i) and the $(i + 1)$st (at temperature T_{i+1}) passes, respectively, while σ_0^i and σ_0^{i+1} are the yield stresses of a fully recrystallized material for the ith and $(i + 1)$st passes. The stresses σ_m^i and σ_y^{i+1} were derived from the pass-to-pass flow curves, while σ_0^i and σ_0^{i+1} were determined from the relationship derived from the values of the yield stresses measured in the stress-strain curves corresponding to the range of complete recrystallization. The yield stresses were determined by the 2 pct offset method.

In addition, experimental T_{nr} values calculated from multipass torsion tests (as reported in Table III) are indicated in Figure 6 (see the results shown in Section III–C–1). Evidently the softening behavior differs depending on the alloy concept. The decrease of softening in the microalloyed steels starts at higher austenite temperatures as expected. While at high temperatures the reduced softening could be related to the solute drag effect, strain induced precipitation in the Nb microalloyed variants becomes the dominating mechanism at lower austenite temperatures.

In general the model predicts the fractional softening behavior reasonably well for the different steel grades. The best match between the model prediction and experimental data is found for the CMnMoNbB steel. For the CMnMoB steel the model overestimates fractional softening below temperatures of approximately 980 °C while it underestimates FS at higher temperatures. The experimental data indicate that solute drag by Mo becomes particularly strong at lower austenite temperatures, potentially supported by precipitation of residual Ti. In the CMnNbB steel the degree of FS is larger than predicted especially at temperatures below T_{nr}. In an earlier study on the same steels it has been observed that dynamic recrystallization can occur in this alloy variant during deformation passes at lower austenite temperatures.[2] Such dynamic recrystallization was however completely suppressed in the CMnNbMoB alloy variant. The present data on the CMnNbMoB alloy variant (Figure 7(d)) support this earlier observation.

The effect of deformation strain and interpass time on the temperature evolution of FS is analyzed for the CMnNbB variant in Figure 7, again comparing predicted and experimental data. For the lower strain of 0.2 complete recrystallization is not even achieved during the initial deformation passes at high austenite temperatures for both interpass times (Figures 7(a) and (c)). The lower strain and thus the reduced driving force cannot sufficiently overcome the Nb solute drag effect preventing complete softening. Clearly, the solute drag effect is strongest for the shorter interpass time. Increasing the strain to 0.3 (Figures 7(b) and (d)), recrystallization approaches completeness for the longer interpass time. Comparing the experimental data to the MicroSim-PM® simulation results, it appears that the model correctly predicts the influence of deformation conditions (strain and interpass time) on the evolution of the austenite fractional softening along the pass schedule.

IV. CONCLUSIONS

The analysis of recrystallization kinetics and double twist torsion test results performed on four different variants of typical direct quenching steel alloy designs indicated that additions of Nb, Mo and Nb + Mo severely delay the softening kinetics at lower deformation temperatures. This is due to increasing solute drag on the austenite grain boundary by segregated alloying elements. Even if the solute drag effect of Nb per unit mass is the highest one, molybdenum has the most pronounced effect due to the higher number of solute atoms with the current compositions.

Nb microalloying shows a dual effect by providing solute drag at higher austenite temperature and grain boundary pinning by strain induced Nb precipitates at lower austenite temperature. The presence of Nb-rich strain induced precipitates has been confirmed by microscopic analysis. The accuracy of an established constitutive equation predicting the time for achieving 50 pct recrystallization was confirmed to be also valid for higher Mo levels used in some of the current steels.

Multipass torsion tests indicated that the solute drag effect is more dominant at shorter interpass time. It diminishes at longer interpass time but clearly less pronouncedly for the molybdenum alloyed variants. The variation of deformation strain also has more influence

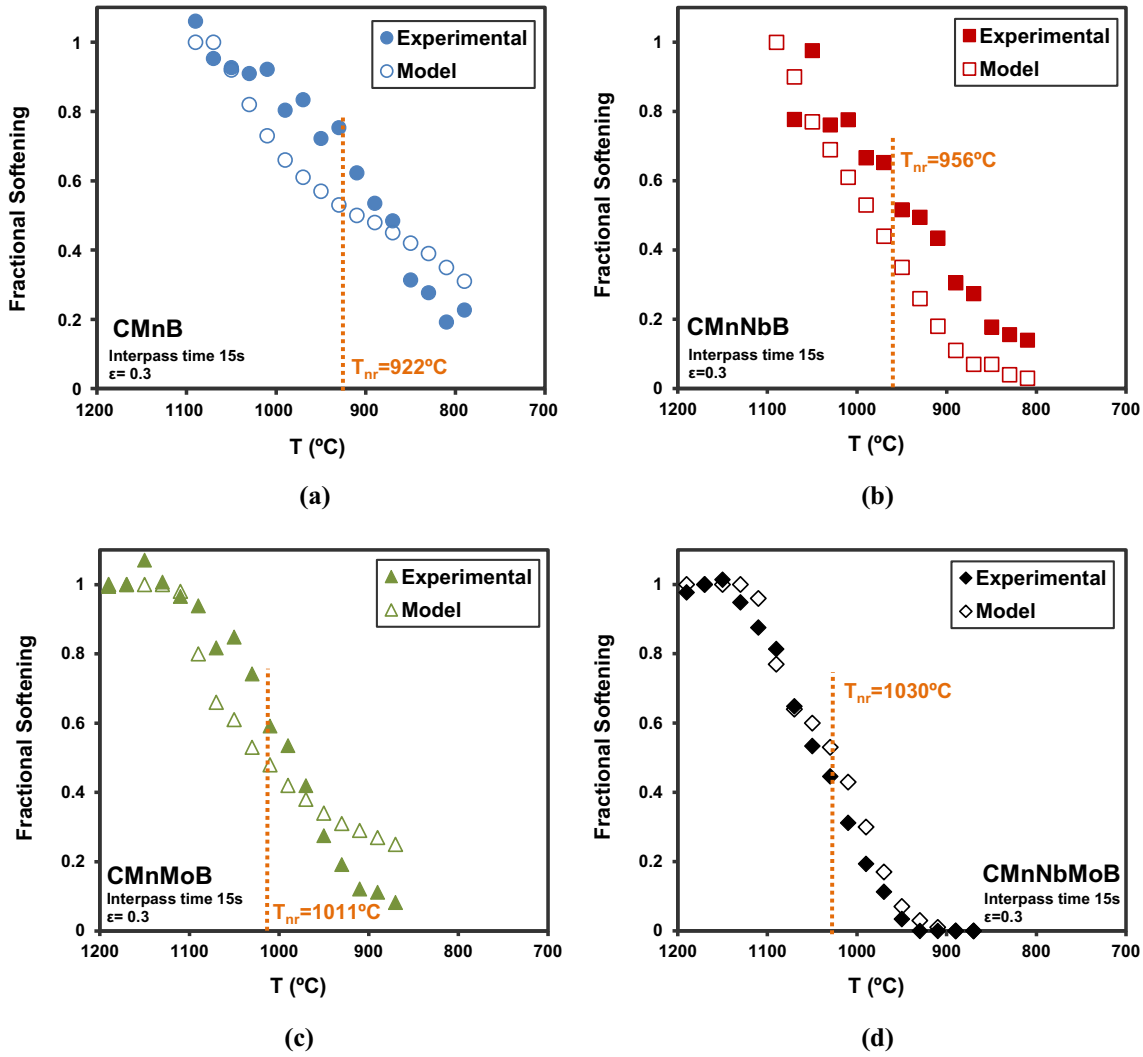

Fig. 6—Comparison between experimental fractional softening curves obtained from multipass torsion tests and those predicted by MicroSim-PM® (interpass time of 15 s and strain of 0.3): (*a*) CMnB, (*b*) CMnNbB, (*c*) CMnMoB and (*d*) CMnNbMoB. Non-recrystallization temperature (T_{nr}) as obtained in Fig. 5 is also indicated.

on the non-recrystallization temperature in the molybdenum alloyed variants. The larger deformation strain had apparently however no significant effect on the strain-induced precipitation of niobium at either interpass time in the present steels.

The combined addition of niobium and molybdenum results in synergetic behavior. At higher austenite temperatures, both niobium and molybdenum exert a strong solute drag effect. At lower austenite temperatures, niobium partially precipitates and in combination with solute drag exerted by molybdenum completely suppresses fractional softening, even under the larger deformation strain and for the longer interpass time.

MicroSim-PM® software was employed for predicting the recrystallized fraction of austenite from pass to pass and estimating the evolution of fractional softening during plate hot rolling simulation. Even though the software was so far mainly used and optimized for standard microalloyed HSLA steels, predictions of fractional softening for the current direct quenching steel alloys showed reasonably good agreement with the experimental behavior. Nevertheless, improvements in the underlying constitutive equations to better account for the austenite grain boundary segregation behavior of molybdenum and boron should be implemented.

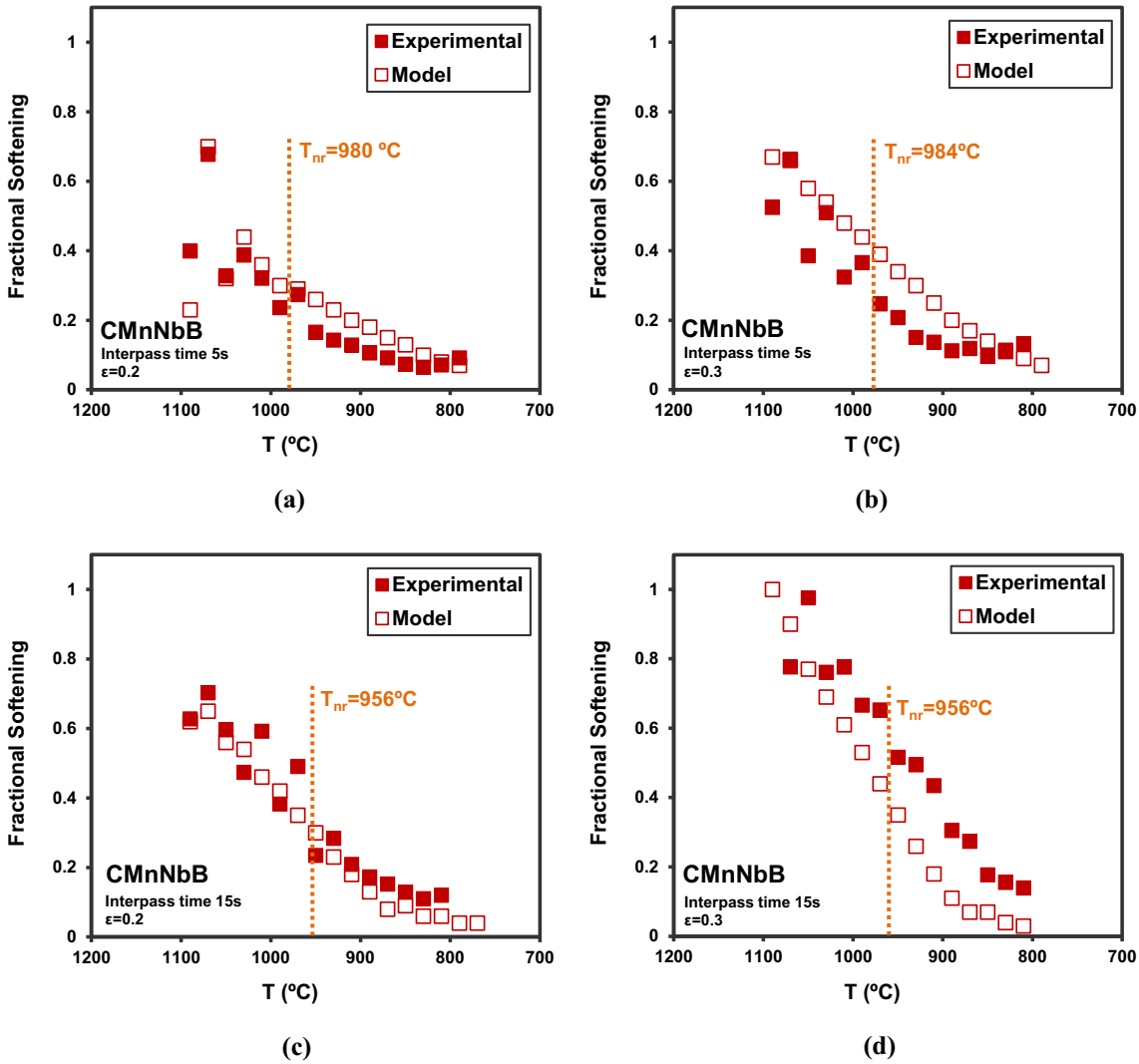

Fig. 7—Comparison between experimental fractional softening curves obtained from multipass torsion tests and predicted by MicroSim-PM® for CMnNbB steel: (*a*) $\varepsilon = 0.2$, $t_{ip} = 5$ s, (*b*) $\varepsilon = 0.2$, $t_{ip} = 15$ s, (*c*) $\varepsilon = 0.3$, $t_{ip} = 5$s and (*d*) $\varepsilon = 0.3$, $t_{ip} = 15$ s. Non-recrystallization temperature (T_{nr}) as obtained in Fig. 5 is also indicated.

ACKNOWLEDGMENTS

The authors would like to acknowledge the International Molybdenum Association (IMOA) for funding this project.

CONFLICT OF INTEREST

The authors declare that they have no conflict of interest.

FUNDING

Open Access funding provided thanks to the CRUE-CSIC agreement with Springer Nature.

REFERENCES

1. I. Zurutuza, N. Isasti, E. Detemple, V. Schwinn, H. Mohrbacher, and P. Uranga: *Metals*, 2021, vol. 11(1), art. no. 29. https://doi.org/10.3390/met11010029.
2. I. Zurutuza, N. Isasti, E. Detemple, V. Schwinn, H. Mohrbacher, and P. Uranga: *Metals*., 2021, vol. 11(1), art. no. 95. https://doi.org/10.3390/met11010095.
3. H. Mohrbacher: *Metals*., 2018, vol. 8(4), art no. 234. https://doi.org/10.3390/met8040234.
4. X.L. He, M. Djahazi, J.J. Jonas, and J. Jackman: *Acta Met. Mater*., 1991, vol. 39(10), pp. 2295–308. https://doi.org/10.1016/0956-7151(91)90012-P.
5. I. Zurutuza, N. Isasti, E. Detemple, V. Schwinn, H. Mohrbacher, and P. Uranga: *JOM*., 2021, vol. 73, pp. 3158–68. https://doi.org/10.1007/s11837-021-04773-0.
6. M.G. Akben, B. Bacroix, and J.J. Jonas: *Acta Metall*., 1983, vol. 31(1), pp. 161–74. https://doi.org/10.1016/0001-6160(83)90076-7.
7. B. Pereda, B. López and J.M. Rodriguez-Ibabe: *Int. Conf. Microalloyed Steels Process Microstruct. Prop. Perform. Proc*., Pittsburgh, PA, USA, July 2007, pp. 151–59.
8. C. Klinkenberg, K. Hulka, and W. Bleck: *Steel Res. Int*., 2004, vol. 75, pp. 746–54. https://doi.org/10.1002/srin.200405837.
9. E.J. Palmiere, C.I. García, and A.J. DeArdo: *Metall. Mater. Trans. A*., 1996, vol. 27A, pp. 951–60. https://doi.org/10.1007/BF02649763.
10. A.I. Fernandez, B. Lopez, and J.M. Rodriguez-Ibabe: *Scripta Mater*., 1999, vol. 40(5), pp. 543–49. https://doi.org/10.1016/S1359-6462(98)00452-7.
11. L. Llanos, B. Pereda, and B. Lopez: *Metall. Mater. Trans. A*., 2015, vol. 46A, pp. 5248–65. https://doi.org/10.1007/s11661-015-3066-2.
12. T.J. Ballard, J.G. Speer, K.O. Findley, and E. De Moor: *Sci. Rep*., 2021, vol. 11, art no. 1495. https://doi.org/10.1038/s41598-021-81139-1.
13. D.Q. Bai, S. Yue, W.P. Sun, and J.J. Jonas: *Metall. Mater. Trans. A*., 1993, vol. 24A, pp. 2151–59. https://doi.org/10.1007/BF02648589.
14. S. Vervynckt: *Control of the Non-Recrystallization Temperature in High Strength Low Alloy (HSLA) Steels*, Ghent University, Ghent, Belgium, 2010. http://hdl.handle.net/1854/LU-4333753.
15. S.F. Medina and A. Quispe: *ISIJ Int*., 2001, vol. 41(7), pp. 774–81. https://doi.org/10.2355/isijinternational.41.774.
16. B. Pereda, J.M. Rodriguez-Ibabe, and B. Lopez: *ISIJ Int*., 2008, vol. 48(10), pp. 1457–66. https://doi.org/10.2355/isijinternational.48.1457.
17. M. Hoerner, J. Speer, and M. Eberhart: *ISIJ Int*., 2017, vol. 57(10), pp. 1847–50. https://doi.org/10.2355/isijinternational.ISIJINT-2017-096.
18. S. Medina and J. Mancilla: *ISIJ Int*., 1996, vol. 36(8), pp. 1063–69. https://doi.org/10.2355/isijinternational.36.1063.
19. M. Akben, T. Chandra, P. Plassiard, and J.J. Jonas: *Acta Metall*., 1984, vol. 32(4), pp. 591–601. https://doi.org/10.1016/0001-6160(84)90070-1.
20. L. Karlsson and H. Norden: *Le J. Phys. Colloq*., 1986, vol. 47(C7), pp. C7-257–62. https://doi.org/10.1051/jphyscol:1986744.
21. J.E. Morral and W.F. Jandeska: *Metall. Mater. Trans. A*., 1980, vol. 11A, pp. 1628–29. https://doi.org/10.1007/BF02654530.
22. W.F. Jandeska and J.E. Morral: *Metall. Trans*., 1972, vol. 3(11), pp. 2933–37. https://doi.org/10.1007/BF02652863.
23. X.L. He, M. Djahazi, J.J. Jonas, and J. Jackman: *Acta Metall. Mater*., 1991, vol. 39(10), pp. 2295–308. https://doi.org/10.1016/0956-7151(91)90012-P.
24. L.J. Cuddy and J.C. Raley: *Metall. Mater. Trans. A*., 1983, vol. 14A, pp. 1989–95. https://doi.org/10.1007/BF02662366.
25. H. Mohrbacher and T. Senuma: *Metals*., 2020, vol. 10(7), art no. 853. https://doi.org/10.3390/met10070853.
26. Y. Li, D. Ponge, P.P. Choi, and D. Raabe: *Scripta Mater*., 2015, vol. 96, pp. 13–16. https://doi.org/10.1016/j.scriptamat.2014.09.031.
27. J. Webel, A. Herges, D. Britz, E. Detemple, V. Flaxa, H. Mohrbacher, and F. Mücklic: *Metals*., 2020, vol. 10(2), art no. 243. https://doi.org/10.3390/met10020243.
28. N. Maruyama, R. Uemori, and M. Sugiyama: *Mater. Sci. Eng. A*., 1998, vol. 250(1), pp. 2–7. https://doi.org/10.1016/S0921-5093(98)00528-0.
29. X. Azpeitia, N. Isasti, P. Uranga, J.M. Rodriguez Ibabe, D.G. Stalheim and M. Rebellato: *Procs. 2nd International Symposium on the Recent Developments in Plate Steels, AIST,* Orlando, FL, 3–6 June, 2018, pp. 83–91.
30. W.J. Liu and M.G. Akben: *Can. Metall. Q*., 1987, vol. 26(2), pp. 145–53. https://doi.org/10.1179/cmq.1987.26.2.145.